Laser transmission through thin cirrus clouds

K. N. Liou, Y. Takano, S. C. Ou, and M. W. Johnson

A near-infrared airborne-laser transmission model for thin cirrus clouds has been developed on the basis of the successive-order-of-scattering approach to account for multiple scattering by randomly and horizontally oriented ice crystals associated with an aircraft–target system. Direct transmission and transmission due to multiple scattering are formulated specifically for this geometric system, in which scattering and absorption associated with aerosols, water vapor, and air are accounted for. A number of sensitivity experiments have been performed for investigation of the effect of aircraft–target position, cirrus cloud optical depth, and ice crystal size on laser transmission for tactical applications. We show that transmission contributions produced by orders of scattering higher than 1 are small and can be neglected. The possibility of horizontal orientation of ice crystals can enhance transmission of laser beams in the aircraft–target geometry. Transmitted energy is strongly dependent on the horizontal distance between the aircraft and the target and on the cloud optical depth as well as on whether the cloud is above or below the aircraft.

OCIS codes: 140.0140, 010.3310, 010.1320, 290.1090.

1. Introduction

In a paper published in this journal, a model for the evaluation of the transmission of emitted infrared radiation from a hot target through thin cirrus was developed.[1] It was pointed out that cirrus clouds, particularly thin cirrus, are globally distributed; they are present at all latitudes and in all seasons, with an average fractional cloud cover of approximately 20–30%. Some of these clouds are subvisual and can interact significantly with radiation by means of long-path transmission. On the basis of observations from ground-based lidar and radar, airborne instrumentations, and satellites, cirrus clouds are typically located in the upper troposphere and the lower stratosphere. The formation, maintenance, and dissipation of these clouds are directly associated with synoptic and mesoscale disturbances as well as being related to deep cumulus outflows. Increases of high cloud cover have been noted at several urban airports in the United States from surface observations spanning 40 years; the increases are attributed to the contrails and water vapor generated by jet airplane traffic.[2,3] Satellite observations from the National Oceanic and Atmospheric Administration's High-Resolution Infrared Radiation Sounder (HIRS) by the CO_2 slicing method also show a substantial increase of cirrus cover over the tropics in recent years.[4] The composition of cirrus varies significantly in time and space. Laboratory and field experiments illustrate that the shape and size of ice crystals in cirrus clouds are governed by temperature and supersaturation, but they normally have a basic hexagonal structure. In the atmosphere, if the growth of ice particles involves collision and coalescence, the shapes of the particles can be extremely complex. Observations from aircraft optical probes and replicator techniques for tropical, midlatitude, and contrail cirrus reveal that these clouds are composed largely of bullet rosettes, solid and hollow columns, single and double plates, aggregates, and ice crystals with irregular surfaces with sizes ranging from a few micrometers to ~1000 μm.

In recent years, high-energy lasers at near-infrared wavelengths have been developed. With advances in laser technology, an active system can be incorporated into the aircraft platform for engagement with a moving target. For such a system to be effective in operation, the atmospheric effects must be carefully taken into consideration. The presence of persistent high-level cirrus in addition to optical turbulence, also can potentially cause concern for the transmission of laser beams from the aircraft position to the target, particularly in the regions of the upper tropo-

K. N. Liou (knliou@atmos.ucla.edu), Y. Takano, and S. C. Ou are with the Department of Atmospheric Sciences, University of California, Los Angeles, Los Angeles, California 90095. M. W. Johnson is with the Airborne Laser Program System Office, Kirtland Air Force Base, New Mexico 87117-6612.

Received 3 December 1999; revised manuscript received 25 May 2000.

0003-6935/00/274886-09$15.00/0

sphere and the lower stratosphere, where most of the thin cirrus clouds reside. In this paper we present a transmission model specifically developed for long-path cw laser transmission through high cirrus clouds. In addition to ice crystals, air molecules, aerosols, and water vapor are also taken into account in the transmission formulations. In Section 2, direct transmission and transmission as a result of multiple scattering are formulated. Computational results with the 1.315-μm laser wavelength are presented in Section 3. A summary is given in Section 4.

2. Formulation of Laser Transmission

A. Direct Transmission

Direct transmission follows exponential attenuation, and the transmitted power F_d can be written in the form

$$F_d = F_0 \exp(-\beta_e s) = F_0 \exp[-(\beta_{\text{air}} + \beta_{\text{aer}} + k_v \rho + \beta_{\text{cld}})s], \quad (1)$$

where F_0 is the laser power in units of watts; the total extinction coefficient β_e is the sum of the scattering coefficient of air molecules β_{air}, the extinction coefficient of aerosols β_{aer}, the absorption coefficient of water vapor times water-vapor density $k_v\rho$, and the extinction coefficient of cirrus cloud particles β_{cld}. The parameter s is a distance along the laser beam between the cloud top and the cloud base, which can be expressed by

$$s = (z_t - z_b)/\mu, \quad (2)$$

where μ is the sine of the scan angle $\theta = \tan^{-1}[(z_a - z_m)/d]$ of the laser beam, as shown in Fig. 1(a); z_a, z_t, z_b, and z_m are the heights of the aircraft, the cloud top, the cloud base, and the target, respectively; and d is the horizontal distance between the aircraft and the target.

B. Multiple-Scattering Contributions to the Transmission Formulation

Our transmission formulation associated with multiple scattering follows the model developed by Liou *et al.*[1] First, transmission that is due to the nth-order scattering can be expressed in the form

$$F^{(n)}(0, \Omega) = \int_0^s J^{(n)}(s', \Omega)\exp(-\beta_e s')\beta_e ds', \quad n = 1, 2, \ldots, \quad (3)$$

where the nth-order source function is defined by

$$J^{(n)}(s', \Omega) = \frac{\tilde{\omega}}{4\pi}\int_{\Delta\Omega} F^{(n-1)}(s', \Omega')P(\Omega', \Omega)d\Omega', \quad (4)$$

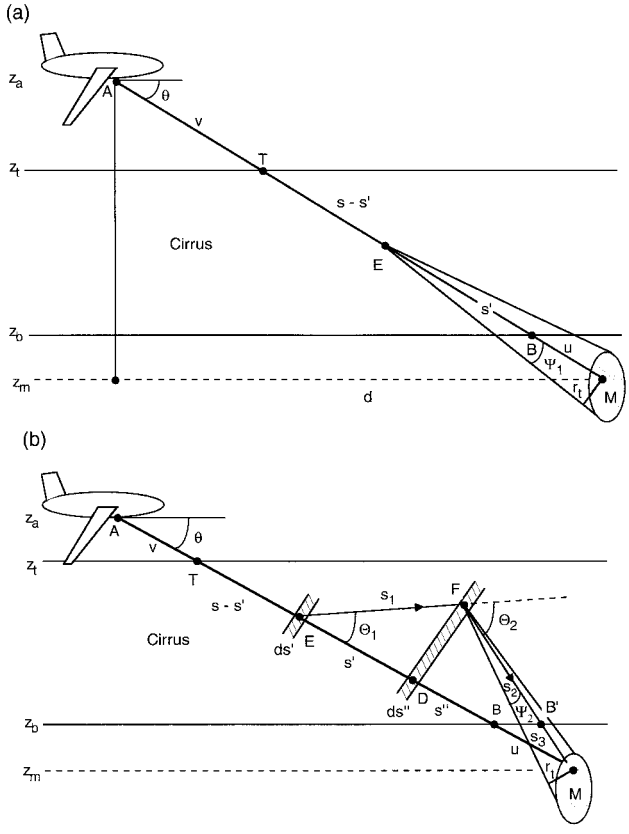

Fig. 1. (a) First-order scattering contribution and definitions of scan angle θ and path length s in an aircraft–target system. $s' = BE$, $s - s' = ET$, $u = BM$, and $v = AT$. (b) Second-order scattering contribution in an aircraft–target system. $s - s' = ET$, $s' = EB$, $s'' = DB$, $u = BM$, $v = AT$, $s_1 = EF$, $s_2 = FB'$, and $s_3 = B'M$.

where $P(\Omega', \Omega)$ is the scattering phase function of the cloud particles, $\tilde{\omega}$ is the single-scattering albedo, and, according to Eq. (1), $F^{(0)}(s', \Omega')$ is given by

$$F^{(0)}(s', \Omega') = F_0 \exp[-\beta_e(s - s')]. \quad (5)$$

In this formulation the laser beam is assumed to be collimated, so no angular width is included in Eq. (5), which differs from that presented by Liou *et al.*[1]; s' is a distance EB along the laser beam between the cloud base and a certain point in the cloud, as shown in Fig. 1. From Eq. (4), the first-order source function $J^{(1)}(s', \Omega)$ can be written in the form

$$J^{(1)}(s', \Omega) = \frac{\tilde{\omega}}{2} F^{(0)}(s', \Omega)\int_0^{\Psi_1} P(\Theta)\sin\Theta d\Theta, \quad (6)$$

where $P(\Theta)$ is the phase function of the cloud, which is a function of scattering angle Θ, and Ψ_1 is an angle associated with the target when it is viewed from point E, which can be expressed by

$$\Psi_1 = \tan^{-1}\left(\frac{r_t}{u + s'}\right), \quad (7)$$

where r_t is the effective radius of the target and $u = (z_b - z_m)/\mu$ is a distance BM between the cloud base

and the target. Finally, from Eq. (3), transmission that is due to first-order scattering can be expressed by

$$F^{(1)}(0, \Omega) = \exp[-(\beta_{\mathrm{nc},a}v + \beta_{\mathrm{nc},b}u)] \int_0^s J^{(1)}(s', \Omega) \times \exp(-\beta_e s')\beta_e \mathrm{d}s'. \quad (8)$$

Exponential attenuation outside the cloud is accounted for in Eq. (8), where $\beta_{\mathrm{nc},a}$ and $\beta_{\mathrm{nc},b}$ are the extinction coefficients that are due to noncloud materials (air molecules, aerosols, and water vapor) above and below the cloud, respectively, and $v = (z_a - z_t)/\mu$ denotes a distance between the aircraft and the cloud top.

In a manner similar to that for first-order scattering, we can determine second-order scattering. Taking into account the specific geometry defined in Fig. 1 and using Eq. (6), we now find the first-order source function $J^{(1)}$ as

$$J^{(1)}(s', \Omega') = \frac{\tilde{\omega}}{2} F^{(0)}(s', \Omega') \int_0^{\Theta_1{}^t} P(\Theta_1)\sin\Theta_1 \mathrm{d}\Theta_1, \quad (9)$$

where $F^{(0)}$ is the direct transmitted component expressed by Eq. (5). The upper limit of scattering angle $\Theta_1{}^t$ is given by the minimum of the two angles as follows:

$$\Theta_1{}^t = \min\left\{\tan^{-1}\left[\frac{(z_t - z_b)\cos\theta}{s' - s''}\right], \tan^{-1}\left[\frac{(z_t - z_b)(1/\cos\theta - \cos\theta)}{s' - s''}\right]\right\}, \quad (10)$$

where s'' is the position at which second-order scattering occurs along the path, as shown in Fig. 1(b). Source function $J^{(1)}$ can now be integrated along the path to give the first-order scattering contribution in the form

$$F^{(1)}(s'', \Omega') = \int_0^s J^{(1)}(s', \Omega')\exp(-\beta_e s_1)\beta_e \mathrm{d}s', \quad (11)$$

where $s_1 = (s' - s'')/\cos\Theta_1$. Next, second-order source function $J^{(2)}(s'', \Omega')$ is given by

$$J^{(2)}(s'', \Omega') = \frac{\tilde{\omega}}{2} \int_{\Theta_2 - \Psi_2}^{\Theta_2 + \Psi_2} F^{(1)}(s'', \Omega') P(\Theta)\sin\Theta \mathrm{d}\Theta, \quad (12)$$

where the relevant angles can be expressed as follows:

$$\Theta_2 = \frac{\pi}{2} + \Theta_1 - \tan^{-1}\left[\frac{s'' + u}{(s' - s'')\tan\Theta_1}\right], \quad (13)$$

$$\Psi_2 = \tan^{-1}\left(\frac{r_t}{s_2 + s_3}\right), \quad (14)$$

$$s_2 + s_3 = \frac{s'' + u}{\cos(\Theta_2 - \Theta_1)}, \quad (15)$$

$$s_3 = \frac{u\sin\theta}{\sin(\theta + \Theta_2 - \Theta_1)}. \quad (16)$$

Finally, transmission that is due to second-order scattering can be expressed by

$$F^{(2)}(0, \Omega') = \exp[-(\beta_{\mathrm{nc},a}v + \beta_{\mathrm{nc},b}s_3)] \int_0^s J^{(2)}(s'', \Omega') \times \exp(-\beta_e s_2)\beta_e \mathrm{d}s''. \quad (17)$$

Note that, when the aircraft is below the cloud and the target is above the cloud, a similar formulation can be derived.

C. Single-Scattering and Absorption Parameters

The computation of laser transmission through clouds and the atmosphere requires knowledge of the single-scattering and absorption parameters involving ice crystals, aerosols, and water vapor associated with the laser wavelengths. In what follows, we describe the data used for these transmission calculations.

In recent years, we have developed a number of light-scattering programs for ice crystals of various shapes and sizes that are typical of those that occur in cirrus clouds. We used a Monte Carlo–geometric-ray-tracing method to compute the scattering, absorption, and polarization properties of large ice particles with several regular and irregular structures, including solid and hollow columns, single and double plates, dendrites, bullet rosettes, and aggregates.[5] The shapes of these ice crystals are defined by appropriate geometric models and incident coordinate systems. The incident photons are traced with a hit-and-miss Monte Carlo method and followed by geometric reflection and refraction on the crystal boundary in which absorption can be accounted for by stochastic procedures. The geometric ray tracing requires a principle of localization such that the particle size is larger than the incident wavelength. In addition, it is assumed that the energy attenuated by the scatterer can be decomposed into equal extinction from diffraction, reflection, and refraction such that the extinction efficiency is equal to 2 regardless of the particle size parameter.

To improve the geometric ray-tracing method we use the innovative approach of mapping the equivalent tangential electric and magnetic fields on the particle surface that are determined by geometric reflection and refraction to the far field by means of the basic electromagnetic wave theory.[6] One can use the improved method to compute the scattering and absorption properties of irregular ice particles with size parameters larger than approximately 15–20. Moreover, we have developed a finite-difference time-domain (FDTD) technique for solution of the problem of light scattering by small ice crystals. It

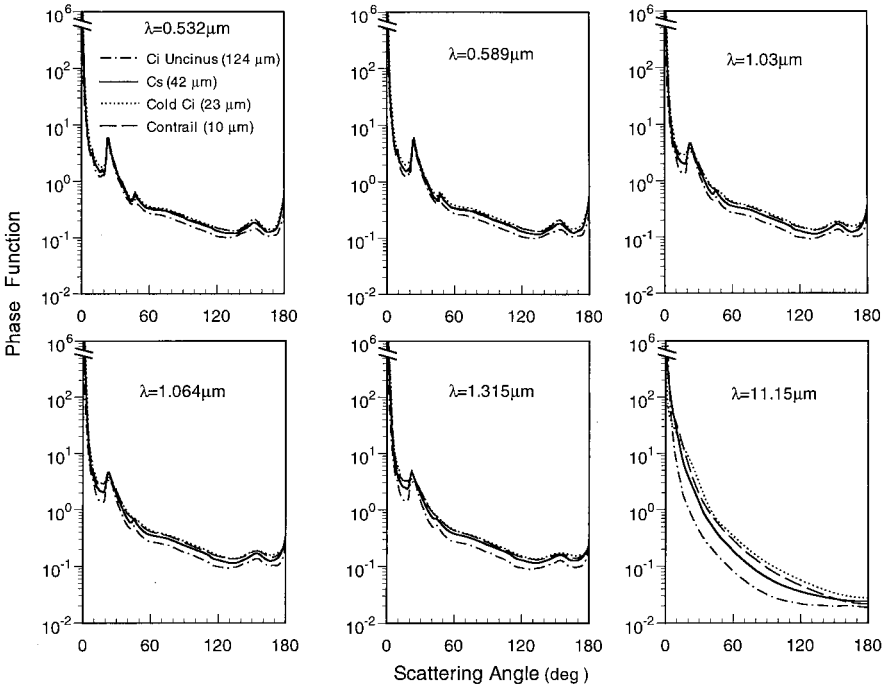

Fig. 2. Phase functions for six laser wavelengths corresponding to four typical cirrus clouds. Ice crystal mean effective sizes D_e for cirrus cloud models are shown in parentheses.

solves the Maxwell equations by using appropriate absorbing boundary conditions and is considered to be exact, as verified by exact Mie results for long circular cylinders and spheres.[7,8] Because of the finite discretization and numerical limitation as well as the computer time requirement, the FDTD method is applicable to size parameters smaller than ~20. By unifying the modified geometric ray-tracing and FDTD methods, we are now in a position to carry out the numerical simulation of light scattering and absorption of ice crystals with arbitrary sizes and shapes that can be defined mathematically or numerically.

The refractive indices for ice that correspond to laser wavelengths are determined by appropriate interpolations of the existing values listed by Liou.[9] We employ four ice crystal size distributions that represent cirrus uncinus, typical cirrostratus, and cold cirrus (abbreviated as Ci Uncinus, Cs, and Cold Ci, respectively, in Figs. 2 and 3) conditions as well as contrail cirrus.[10] Based on the available ice crystal size distribution observations, we use a cirrus model consisting of a combination of bullet rosettes and aggregates (50%), hollow columns (30%), and plates (20%). When we have defined the refractive indices for ice, the ice crystal size distributions, and the shape model, we can carry out the scattering and absorption calculations by using the programs described above. For ice crystals with size parameters smaller than 20, the FDTD method is used in the calculations, whereas for those with size parameters larger than 20 the modified geometric ray-tracing method is followed.

Single-scattering properties for six laser wavelengths (λ = 0.532, 0.589, 1.03, 1.064, 1.315, 11.15 μm) are computed from a combination of the FDTD and geometric ray-tracing methods.[11] Figure 2 shows the phase functions for the six wavelengths. Except for the 11.15-μm wavelength, we see the typical halo patterns at the 22° and 46° scattering angles associated with the hexagonal structure of ice crystals. The diffraction peak at forward-scattering angles varies when the mean effective ice crystal size changes, even though it cannot be distinguished in the figure. The mean effective ice crystal size D_e is defined in terms of the maximum dimension D in the form

$$D_e = \int Vn(D)\mathrm{d}D \Big/ \int An(D)\mathrm{d}D, \tag{18}$$

where V and A are the volume and the projection area of an ice crystal, respectively. Figure 3 shows the extinction coefficient, the single-scattering albedo, and the asymmetry factor corresponding to those in Fig. 2. The extinction coefficient for cirrus uncinus is much larger than that of the other three cirrus clouds because of its larger mean size. The single-scattering albedo for the first five wavelengths is close to 1 because of the small imaginary refractive index of ice. The asymmetry factor varies only slightly in the near-infrared wavelength region. The asymmetry factor was recently measured by Gerber *et al.*[12] with a 0.63-μm laser beam for aggregate ice particles that occurred in arctic ice clouds. The result is shown in Fig. 3, along with a corresponding theoretical interpretation. Note that these results differ from those computed for

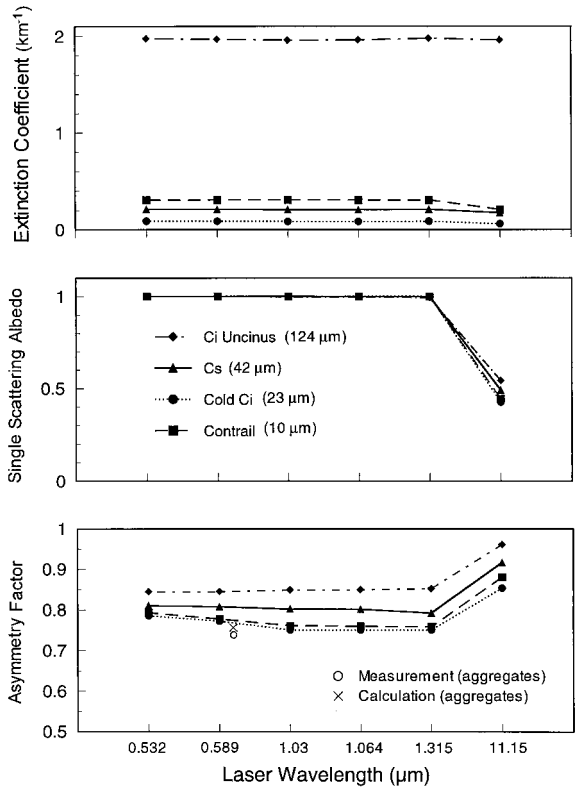

Fig. 3. Extinction coefficients, single-scattering albedos, and asymmetry factors that correspond to the phase functions depicted in Fig. 2. Also included are a measured asymmetry factor at 0.63 μm taken from Ref. 12 for aggregates that occur in arctic ice clouds and a corresponding theoretical interpretation.

the cirrus cloud models that employ a combination of ice crystal shapes.

For ice particles, because of their hexagonal structure, transmission through the two parallel planes of columns and plates can enhance forward scattering. For visible wavelengths this transmission is ~10% of the total transmission[13] and must be accounted for in the scattering calculations. The delta-function transmission part of the extinction coefficient can be computed by means of the similarity principle and can be expressed by $\beta_{cld}\tilde{\omega}f_\delta$, where f_δ is the fractional energy that resides in the forward direction of the phase function.

We have used the standard aerosol (IHAZE = 1) of the MODTRAN3.7 program[14] to define the extinction coefficient of aerosol β_{aer}. However, only the extinction coefficient of aerosols at a wavelength of 0.5 μm is available in MODTRAN. D'Almeida *et al*. have listed the extinction coefficients, single-scattering albedos, and asymmetry factors of 10 aerosol models for 60 wavelengths.[15] The spectral properties of a rural aerosol model are used to interpolate the single-scattering properties of aerosols for the laser wavelengths. We then utilize the MODTRAN standard aerosol model to perform the interpolation necessary to obtain the required vertical resolution for the single-scattering properties of aerosols in the transmission computation. The extinction coefficient of air molecules can be parameterized and is given by

$$\beta_{air} = \frac{\tau_{air}}{\Delta z} = 0.008569\lambda^{-4}(1 + 0.0113\lambda^{-2} + 0.00013\lambda^{-4}) \times \frac{\Delta p}{\Delta z p_0}, \quad (19)$$

where Δz is the thickness of a layer whose pressure difference is Δp, p_0 is 1013.25 mbars, and λ is the wavelength in micrometers.

Water-vapor absorption is treated by means of the correlated *k*-distribution (CKD) method. In the CKD method, the wave-number integration is transformed into an integration over cumulative probability *g*, a monotonically increasing and smooth function in the absorption coefficient space. The use of the *g* function circumvents the requirement of resolving the individual line structures, which are strongly dependent on pressure. The CKD method is exact in the limits of weak- and strong-line approximations, as well as for a single line and for lines with periodic occurrence.[16] Based on this method, only a few integration points are required for an acceptable level of accuracy to be achieved in the transmittance calculations for inhomogeneous atmospheres. We used the CKD method to compute the absorption coefficient of water vapor based on the HITRAN92 line-by-line database.[17] We employed a spectral resolution of 50 cm^{-1} involving 10 *g* to determine the correlated *k* coefficients, following the method developed by Liou *et al*.[10] We incorporated the absorption that is due to water vapor into the scattering process by modifying the extinction coefficient and the single-scattering albedo associated with cloud and aerosol particles.

3. Computational Results

In what follows, we present illustrative results computed from the transmission model. Inputs to the transmission model include the geometric variables that involve the laser beam and the target as well as the single-scattering and absorption parameters for cirrus clouds, aerosols, and water vapor. Background aerosols and water-vapor profiles are assumed for the purpose of this study. However, to evaluate the attenuation of laser energy through high cirrus clouds requires that the information on cloud height, horizontal extent, and ice water content in terms of the effective optical depth be given *a priori*. We envisage that a combination of data sources based on satellite remote sensing and mesoscale model predictions could provide the required information for transmission calculations.

Consider the aircraft above a cirrus cloud and a target at any altitude. Figure 4 shows the transmitted power of the 1.315-μm laser beam (or transmission) as a function of target height z_m. In this calculation a cirrostratus cloud with a mean effective

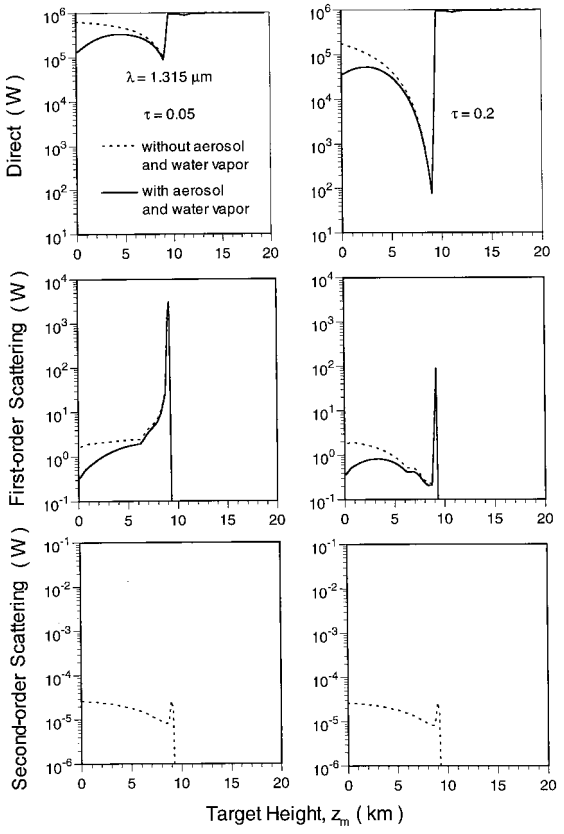

Fig. 4. Direct transmission and transmission owing to first- and second-order scattering through cirrus clouds in the US1976 standard atmosphere as a function of target height z_m. The parameters used in the calculation are $\lambda = 1.315$ μm, $D_e = 42$ μm, $F_0 = 10^6$ W, $r_t = 3$ m, and $d = 100$ km. The cirrus cloud is located between $z_t = 9.5$ and $z_b = 9$ km, and the position of the aircraft, z_a, is 11 km.

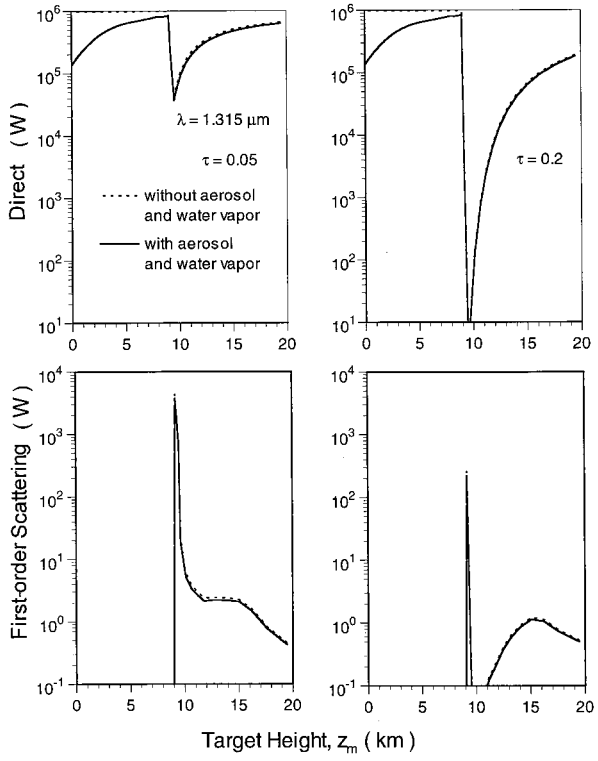

Fig. 5. Same as Fig. 4 but with the position of the aircraft set at $z_a = 8$ km; second-order scattering results are not shown.

ice crystal size of 42 μm is used, along with the standard atmospheric profile. The cloud is located between $z_b = 9$ km and $z_t = 9.5$ km. Other relevant parameters are as follows: laser power, $F_0 = 10^6$ W; effective radius of the target, $r_t = 3$ m; aircraft height, $z_a = 11$ km; horizontal distance between the aircraft and the target, $d = 100$ km; and cirrus optical depth, τ. When aerosols and water vapor in the atmosphere are neglected, the direct transmission decreases with an increase of z_m owing to the longer path lengths inside the cirrus cloud, as shown by the dashed curves in the top two parts of Fig. 4, until the target reaches the cloud base. If aerosols and water vapor are added to the atmosphere, enhanced attenuation near the ground occurs because of their higher mixing ratios there, as shown by the solid curves in the same parts of the figure. After the target emerges from the cloud, the laser beam suffers almost no attenuation. However, when z_m reaches z_t (=11 km), there is a slight decrease in the direct transmission produced by water-vapor absorption associated with the longest path length. When the cloud's optical depth is 0.05, transmission that is due to first-order scattering increases with an increase of z_m owing to the small optical depth, as indicated in the two middle parts of the figure. When the cloud optical depth is 0.2, transmission associated with first-order scattering decreases with an increase of z_m, corresponding to the enhanced attenuation of the direct transmission as displayed at the top of the figure. When the target is inside the cloud, transmission associated with first-order scattering is enhanced by more than 2 orders of magnitude as a result of the contribution from scattering by the diffracted light beam. In general, transmission that is due to first-order scattering is relatively small compared with direct transmission. Transmission produced by second-order scattering is much smaller than the direct component and can be safely neglected.

Figure 5 shows laser transmission for the same configuration as in Fig. 4, except that now the aircraft is below the cloud ($z_a = 8$ km). When the target is between the surface ($z_m = 0$ km) and the cloud base ($z_m = 9$ km), the direct transmission increases monotonically because of the decrease in the aerosol and water-vapor concentrations between the aircraft and the target. Transmission that is due to first-order scattering can be neglected. When the target enters the cloud, the direct transmission decreases abruptly. After the target emerges from the cloud top, the direct transmission increases because of the shorter path lengths in the cloud. Transmission that is due to first-order scattering is almost symmetrical with respect to that displayed in Fig. 4 because of geometrical symmetry. Figure 6 shows laser transmission with the same configuration as in Fig. 4, except that

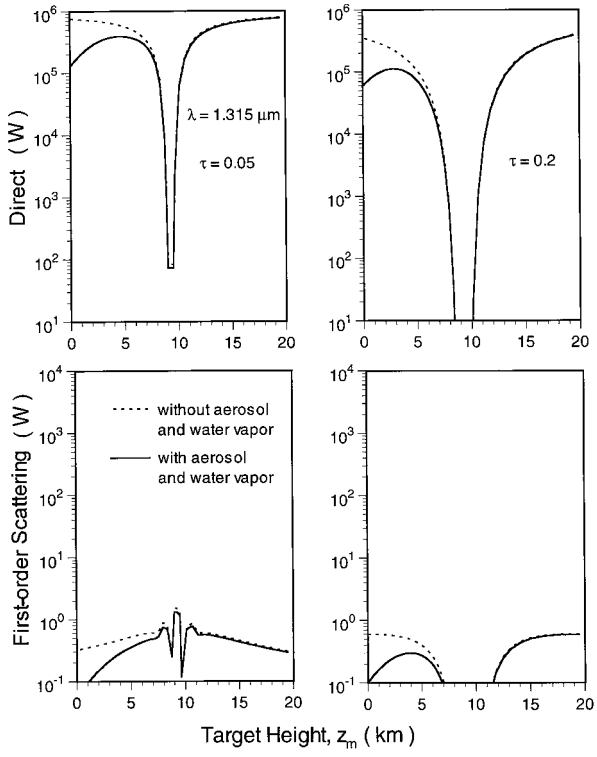

Fig. 6. Same as Fig. 5 but with the position of the aircraft set at $z_a = 9.25$ km. This is an in-cloud configuration.

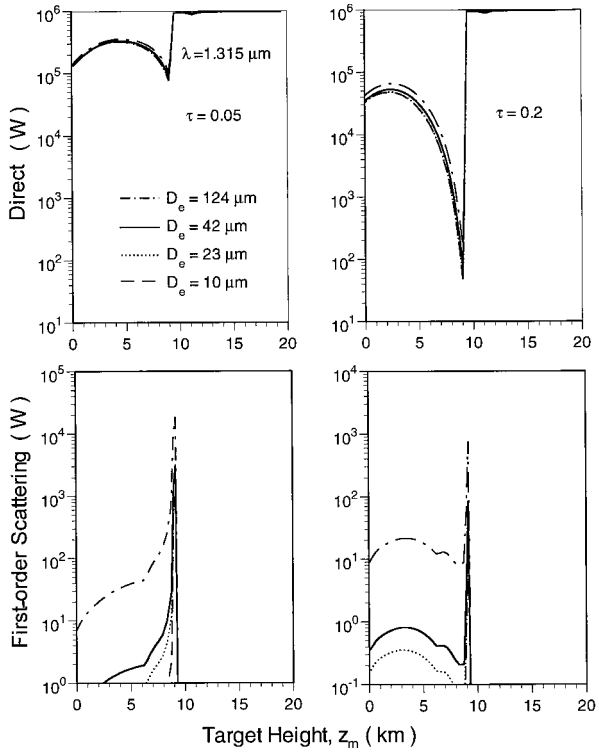

Fig. 7. Direct transmission and transmission owing to first-order scattering through cirrus clouds for several ice crystal mean effective sizes as a function of target height z_m. The parameters used are the same as in Fig. 4. Aerosols and water vapor are included in the calculation.

now the aircraft is inside the cirrus cloud ($z_a = 9.25$ km). In this case, the direct transmission in the top of Fig. 6 is small because of the long path lengths inside the cloud. Correspondingly, transmission that is due to first-order scattering in the bottom of Fig. 6 is also small, unlike in the previous cases. When the target is outside the cloud, the direct transmission increases because of the shorter path lengths in the cloud. If aerosols and water vapor are neglected, the direct transmission and transmission curves associated with first-order scattering are symmetric near $z_m = z_a$ (=9.25 km) because of the symmetric geometric configuration.

In Fig. 7 we investigate the effects of mean effective ice crystal size D_e on laser transmission. We use the same configuration as in Fig. 4. The direct transmission at the top of the figure depends only slightly on D_e. This weak dependence is a result of the delta-function transmission f_δ, which increases when D_e increases. Transmission that is due to first-order scattering depends significantly on D_e because the diffraction peak is more nearly confined to forward-scattering directions for large D_e.

Next, we study the effects of ice crystal horizontal orientation on laser transmission. Figure 8 shows extinction coefficient β_e, single-scattering albedo $\tilde{\omega}$, and delta-function transmission f_δ for horizontally oriented ice crystals as a function of θ, where θ is the emergent angle of the light beam. These parameters are computed from the geometrical-optics approach.[5,17] We consider horizontally oriented columns (referred to as Parry columns) with a size of $L/2a = 300/100$ (μm) and plates (referred to as 2-D plates) with a size of $L/2a = 20/200$ (μm), where L is the maximum dimension and a is the half-width. Although the single-scattering albedo is almost constant, the extinction coefficient and the delta-function transmission tend to increase with an increase of θ. Using $\beta_e(\mu)$, $\tilde{\omega}(\mu)$, and $f_\delta(\mu)$ in Fig. 8 that have the same average values $\bar{\beta}_e$, $\bar{\tilde{\omega}}$, and $\bar{f}_\delta$ as those of the randomly oriented ice crystals defined in Fig. 4, we computed the transmission of a laser beam; the results are shown in Fig. 9. The direct transmission for horizontally oriented ice crystals is larger than that for randomly oriented ice crystals, as shown at the top of Fig. 9, because the relative extinction coefficient in Fig. 8 is smaller than 1 at $\theta < 10°$ for the present aircraft–target geometry. Because of the effect of horizontal orientation, transmission produced by first-order scattering is smaller for $\tau = 0.05$ but more intense for $\tau = 0.2$, the former because of the smaller optical depth for horizontally oriented ice crystals and the latter because there is less attenuation of the direct transmission as displayed at the top of the figure.

4. Summary

A near-infrared laser transmission model involving thin cirrus clouds has been developed for an aircraft–target system, primarily for tactical applications. Transmission produced by multiple scattering is

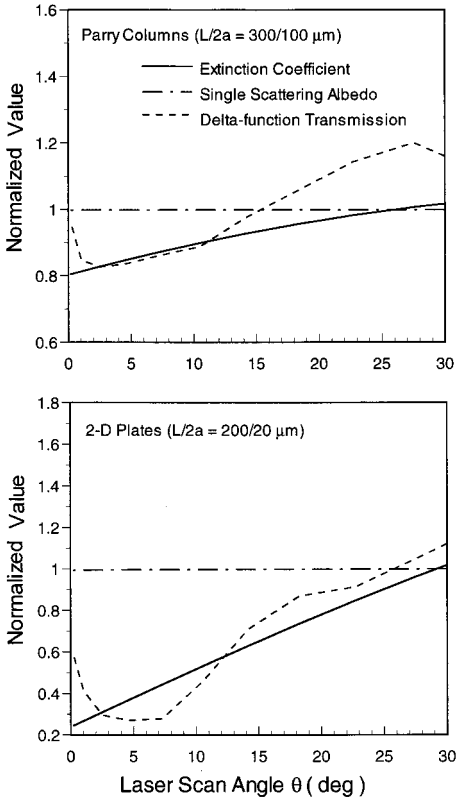

Fig. 8. Normalized extinction coefficient, single-scattering albedo, and delta-function transmission for Parry columns and two-dimensional (2-D) plates as a function of the laser scan angle θ at a wavelength of 1.315 μm.

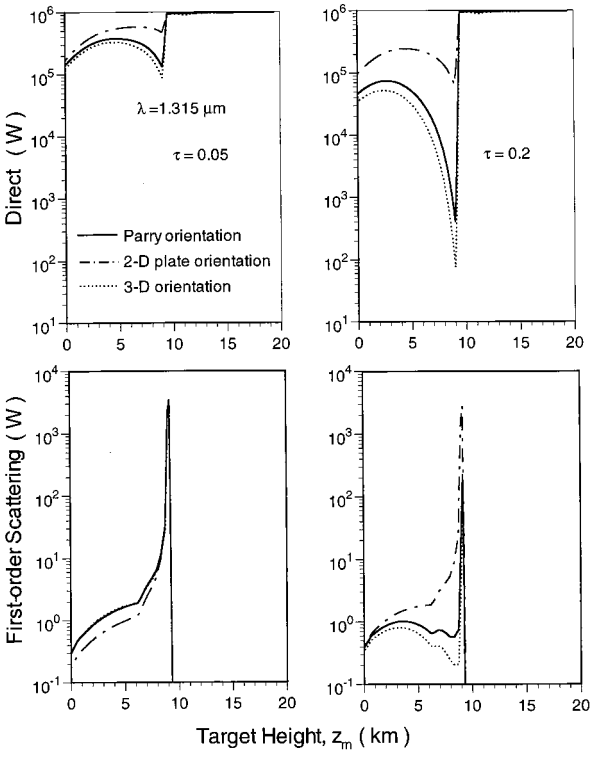

Fig. 9. Direct transmission and transmission owing to first-order scattering through cirrus clouds for horizontally and randomly oriented ice crystals in the US1976 standard atmosphere. The parameters used are the same as in Fig. 4. 2-D and 3-D, two- and three-dimensional, respectively.

evaluated by means of the successive-order-of-scattering procedure in addition to direct transmission. Aerosols, water vapor, and air molecules in the atmosphere are also accounted for in the transmission computation. Transmission that is due to multiple scattering is generally small compared with direct transmission. The sensitivity of laser transmission to aircraft height, cirrus cloud optical depth, laser wavelength, and ice crystal size and orientation was examined with the 1.315-μm laser wavelength. When the target is near the ground, attenuation of the laser beam as a result of the presence of aerosols and water vapor cannot be neglected. Transmitted laser energy in a cirrus cloudy atmosphere is a function of numerous parameters that involve the aircraft's position relative to the cloud, the horizontal distance between the aircraft and the target, the position of the target, the cloud cover, thickness, and composition, and the water-vapor and aerosol profiles. Further, the possibility of ice crystal horizontal orientation is accounted for in the transmission model. We show that the horizontal orientation of ice crystals will make cirrus clouds less opaque because they have smaller extinction coefficients, thus permitting more laser energy to be transmitted. Finally, if we set the aircraft height at 0 km, the present model and analysis can be directly applied to a ground-based laser.

This research has been supported by U.S. Air Force Office of Scientific Research grant F49620-98-1-0232.

References

1. K. N. Liou, Y. Takano, S. C. Ou, A. Heymsfield, and W. Kreiss, "Infrared transmission through cirrus clouds: a radiative model for target detection," Appl. Opt. **29,** 1886–1896 (1990).
2. K. N. Liou, S. C. Ou, and G. Koenig, "An investigation on the climatic effect of contrail cirrus," in *Air Traffic and the Environment—Background, Tendencies and Potential Global Atmospheric Effects*, U. Schumann, ed. (Springer-Verlag, Berlin, 1990), pp. 154–169.
3. D. Frankel, K. N. Liou, S. C. Ou, D. P. Wylie, and W. P. Menzel, "Observation of cirrus cloud extent and their impacts to climate," in *Proceedings of the Ninth Conference on Atmospheric Radiation* (American Meteorological Society, Boston, Mass., 1997), pp. 414–417.
4. D. P. Wylie, W. P. Menzel, H. M. Woolf, and K. I. Strabala, "Four years of global cirrus cloud statistics using HIRS," J. Climate **7,** 1972–1986 (1994).
5. Y. Takano and K. N. Liou, "Radiative transfer in cirrus clouds. III. Light scattering by irregular ice crystals," J. Atmos. Sci. **52,** 818–837 (1995).
6. P. Yang and K. N. Liou, "Geometric-optics integral-equation method for light scattering by nonspherical ice crystals," Appl. Opt. **35,** 6568–6584 (1996).
7. P. Yang and K. N. Liou, "Finite-difference time-domain method for light scattering by small ice crystals in three-dimensional space," J. Opt. Soc. Am. A **13,** 2072–2085 (1996).
8. P. Yang and K. N. Liou, "An efficient algorithm for truncating spatial domain in modeling light scattering by finite-difference technique," J. Comput. Phys. **140,** 346–369 (1998).

9. K. N. Liou, *Radiation and Cloud Processes in the Atmosphere: Theory, Observation, and Modeling* (Oxford U. Press, Oxford, 1992).
10. K. N. Liou, P. Yang, Y. Takano, K. Sassen, T. P. Charlock, and W. P. Arnott, "On the radiative properties of contrail cirrus," Geophys. Res. Lett. **25,** 1161–1164 (1998).
11. K. N. Liou, Y. Takano, and P. Yang, "Light scattering and radiative transfer in ice crystal clouds: applications to climate research," in *Light Scattering by Nonspherical Particles: Theory, Measurements, and Geophysical Applications*, M. I. Mishchenko, J. W. Hovenier, and L. D. Travis, eds. (Academic, New York, 1999), Chap. 15.
12. H. Gerber, Y. Takano, T. J. Garret, and P. V. Hobbs, "Nephelometer measurements of the asymmetry parameter, volume extinction coefficient and backscatter ratio in arctic clouds," J. Atmos. Sci. (to be published).
13. Y. Takano and K. N. Liou, "Solar radiative transfer in cirrus clouds. I. Single-scattering and optical properties of hexagonal ice crystals," J. Atmos. Sci. **46,** 3–19 (1989).
14. G. P. Anderson, R. H. Picard, and J. H. Chetwynd, "Proceedings of the 17th Annual Review Conference on Atmospheric Transmission Models," Special Rep. 274 (Phillips Laboratory/ Geophysics Directorate, Hanscom Air Force Base, Mass., 1995).
15. G. A. d'Almeida, P. Koepke, and E. P. Shettle, *Atmospheric Aerosols: Global Climatology and Radiative Characteristics* (Deepak, Hampton, Va., 1991).
16. Q. Fu and K. N. Liou, "On the correlated k-distribution method for radiative transfer in nonhomogeneous atmospheres," J. Atmos. Sci. **49,** 2139–2156 (1992).
17. L. S. Rothman, R. R. Gamache, R. H. Tipping, C. P. Rinsland, M. A. H. Smith, D. C. Benner, V. M. Devi, J.-M. Flaud, C. Camy-Peyret, A. Perrin, A. Goldman, S. T. Massie, L. R. Brown, and R. A. Toth, "The HITRAN molecular database: editions of 1991 and 1992," J. Quant. Spectrosc. Radiat. Transfer **48,** 469–507 (1992).
18. Y. Takano and K. N. Liou, "Transfer of polarized infrared radiation in optically anisotropic media: application to horizontally oriented ice crystals," J. Opt. Soc. Am. A **10,** 1243–1256 (1993).